RESEARCH ARTICLE

Metastable Intermediates as Stepping Stones on the Maturation Pathways of Viral Capsids

Giovanni Cardone,[a]* Robert L. Duda,[b] Naiqian Cheng,[a] Lili You,[a] James F. Conway,[c] Roger W. Hendrix,[b] Alasdair C. Steven[a]

Laboratory of Structural Biology Research, National Institute of Arthritis, Musculoskeletal and Skin Diseases, Bethesda, Maryland, USA[a]; Department of Biological Sciences, University of Pittsburgh, Pittsburgh, Pennsylvania, USA[b]; Department of Structural Biology, University of Pittsburgh School of Medicine, Pittsburgh, Pennsylvania, USA[c]

* Present address: Giovanni Cardone, Department of Chemistry and Biochemistry, University of California, La Jolla, California, USA.

ABSTRACT **As they mature, many capsids undergo massive conformational changes that transform their stability, reactivity, and capacity for DNA. In some cases, maturation proceeds via one or more intermediate states. These structures represent local minima in a rich energy landscape that combines contributions from subunit folding, association of subunits into capsomers, and intercapsomer interactions. We have used scanning calorimetry and cryo-electron microscopy to explore the range of capsid conformations accessible to bacteriophage HK97. To separate conformational effects from those associated with covalent cross-linking (a stabilization mechanism of HK97), a cross-link-incompetent mutant was used. The mature capsid Head I undergoes an endothermic phase transition at 60°C in which it shrinks by 7%, primarily through changes in its hexamer conformation. The transition is reversible, with a half-life of ~3 min; however, >50% of reverted capsids are severely distorted or ruptured. This observation implies that such damage is a potential hazard of large-scale structural changes such as those involved in maturation. Assuming that the risk is lower for smaller changes, this suggests a rationalization for the existence of metastable intermediates: that they serve as stepping stones that preserve capsid integrity as it switches between the radically different conformations of its precursor and mature states.**

IMPORTANCE **Large-scale conformational changes are widespread in virus maturation and infection processes. These changes are accompanied by the release of conformational free energy as the virion (or fusogenic glycoprotein) switches from a precursor state to its mature state. Each state corresponds to a local minimum in an energy landscape. The conformational changes in capsid maturation are so radical that the question arises of how maturing capsids avoid being torn apart. Offering proof of principle, severe damage is inflicted when a bacteriophage HK97 capsid reverts from the (nonphysiological) state that it enters when heated past 60°C. We suggest that capsid proteins have been selected in part by the criterion of being able to avoid sustaining collateral damage as they mature. One way of achieving this—as with the HK97 capsid—involves breaking the overall transition down into several smaller steps in which the risk of damage is reduced.**

Received 1 October 2014 **Accepted** 20 October 2014 **Published** 11 November 2014

Citation Cardone G, Duda RL, Cheng N, You L, Conway JF, Hendrix RW, Steven AC. 2014. Metastable intermediates as stepping stones on the maturation pathways of viral capsids. mBio 5(6):e02067-14. doi:10.1128/mBio.02067-14.

Editor Terence S. Dermody, Vanderbilt University School of Medicine

Address correspondence to Alasdair C. Steven, stevena@mail.nih.gov.

This article is a direct contribution from a Fellow of the American Academy of Microbiology.

Maturation is the final phase of virus assembly in which a noninfectious precursor particle is transformed to an infectious virion. In this sense, maturation is comparable to enzyme activation but takes place on a larger scale and is usually irreversible. An essential feature of numerous viral systems (e.g., see references 1 to 4), maturation generally involves conformational changes within the viral particle. These changes are triggered—in many but not all systems—by limited proteolysis of the capsid proteins.

Maturation has been studied in depth for the capsids of tailed bacteriophages and their evolutionary codescendants, herpesviruses (5). Capsid maturation by itself does not confer infectivity, but it is a prerequisite for infectivity. The bacteriophage precursor particle (procapsid) expands by about 20% in diameter, and its shape changes from round to polyhedral, with thinner walls and flatter facets. The expansion results in an approximate doubling of its capacity for DNA. Maturation also stabilizes the capsid, enabling it to resist the outward pressure of densely packaged DNA. Stabilization can be effected by any of several molecular mechanisms, depending on the virus: creation of binding sites for clamping proteins that bridge the intercapsomer interfaces (e.g., T4 [6, 7] and lambda [8, 9]), formation of covalent cross-links between adjacent subunits (e.g., HK97 [10]), or simply switching to a stronger set of intermolecular interactions (e.g., P22 [11, 12] and T7 [13]).

Although they employ a variety of stabilization mechanisms, the capsid proteins of tailed bacteriophages share a fold, first visualized in the case of HK97 (14). Essentially the same fold is reproduced in all such viruses studied to date, despite the absence of sequence similarity and the diversity of hosts. It also appears to

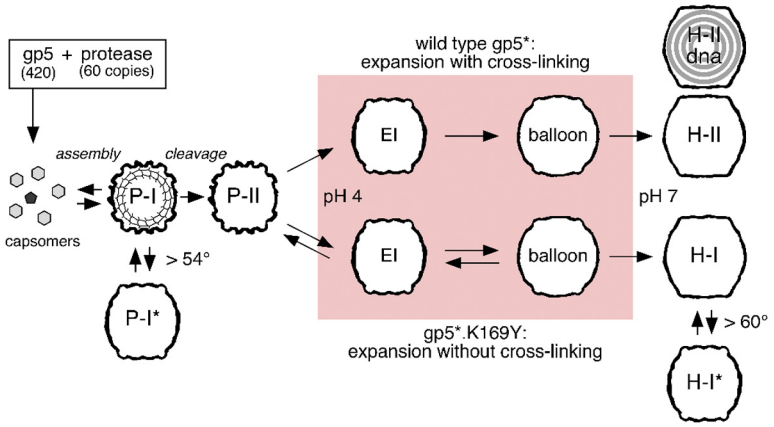

FIG 1 Cartoon outlining the assembly and maturation pathway of the HK97 capsid, both for the wild-type capsid protein gp5 (cleaved form, gp5*), which undergoes cross-linking, and for the K169Y mutant, which cannot cross-link. The wild-type EI was originally thought to consist of two subclasses (14) but is now perceived as a somewhat heterogeneous population in which the particles exhibit various amounts of cross-linking. Head I and Head II are approximately 20% larger than Prohead I or II. EI, Head I*, and Prohead I* are similar in size, about halfway between the two extremes, but they differ structurally in some local features. The capsid of the DNA-filled head is slightly but significantly different from empty Head II, having flatter facets (52).

be adopted by the capsid "floor" domain of herpesviruses (15, 16), animal viruses whose capsids share many structural properties and maturation-related behaviors with phage capsids (5, 17).

HK97 maturation has been particularly amenable to study because the procapsid can be assembled by simply expressing the gene that codes for the capsid protein, gp5 (42 kDa), with or without coexpression of the viral protease (18), and subsequent steps in the maturation pathway may be induced *in vitro* (14, 19, 20). The pathway is outlined in Fig. 1. Detailed structures have been determined for most of these conformations by X-ray crystallography and/or cryo-electron microscopy (cryo-EM) (21). Moreover, possible pathways of maturation have been explored theoretically by molecular dynamics calculations (22). In the first step toward maturation, the precursor capsid protein gp5 (42 kDa) is cleaved to gp5* (31 kDa) by removal of its N-terminal Δ-domain. This converts Prohead I to the metastable Prohead II, whose gp5* shell is only subtly different from that of Prohead I but is primed for expansion (23). *In vivo*, expansion is coupled with and probably driven by DNA packaging; *in vitro*, it may be induced by manipulating the pH. Acidification to pH ~4 followed by reneutralization leads the maturing capsid through two intermediates, called Expansion Intermediate (EI) and Balloon, to the end state, Head II (14, 24). Covalent cross-linking, an autocatalytic process, starts at the EI stage and is completed in Head II. The same structural changes take place in the absence of cross-linking with the K169Y mutant in which a cross-linking lysine is replaced with a cross-linking-incompetent tyrosine. Why there should be metastable icosahedrally symmetric intermediates along a maturation pathway—three of them in the case of HK97, when Prohead II is included (Fig. 1)—has not been clear. A possible answer emerged in the course of this study.

The energetic basis of HK97 capsid maturation has been investigated by combining scanning calorimetry with cryo-electron microscopy to study purified capsids in various conformational states (25, 26). Each kind of capsid denatures at a distinctive melting temperature (T_m). These observations formed the basis for the "free energy cascade" hypothesis, whereby the maturation pathway is envisaged as passing through a sequence of progressively lower local minima in the free energy landscape (26). However, some of the thermograms show additional endothermic events at temperatures lower than the T_m. These transitions are reversible and represent phase transitions of the capsid, typically involving input of 5 to 10% of the heat (enthalpy) required for denaturation (ΔH_m). The 54° endotherm of Prohead I, producing Prohead I*, represents switching to a state in which the gp5 pentamers retain their original conformation while the hexamers switch to their EI state, with their Δ-domains disordered (27), bypassing their Prohead II conformation. Here, we have applied a similar approach to characterize the 60° endotherm of Head I. Our goal was to further explore the range of conformational states accessible to the gp5* capsid, thereby to illuminate the maturation pathways of HK97 and other viral capsids.

RESULTS

When purified Head I is thermally scanned in our standard buffer (near-neutral pH, moderate ionic strength; see Materials and Methods), it registers an endothermic event that peaks at 60°C and is over by 63°C (see Fig. 3 of reference 25). The onset of thermal denaturation comes later at 77°C, peaking at 81°C. In order to capture Head I in its supra-60° conformation (Head I*), we incubated drops of specimen mounted on EM grids at 65°C or 70°C for 10 min (consistent results were obtained with both temperatures) and then vitrified them for observation by cryo-EM. This was done as rapidly as possible to minimize the risk of reversion, i.e., failing to capture the thermally excited state. Because aqueous drops evaporate rapidly at elevated temperatures, these experiments were performed using an environmental chamber in which humidity and temperature could be controlled. We estimate the interval from the specimen being at incubation temperature to its being immobilized in vitreous ice to be a fraction of a second (~0.1 to 0.3 s) (27).

A cryo-electron micrograph of a typical field of heated capsids is shown in Fig. 2A and compared with the starting material in Fig. 2B. The heated capsids are markedly smaller and rounder and have thicker walls than Head I. These features are indicative of a concerted conformational change in the surface lattice.

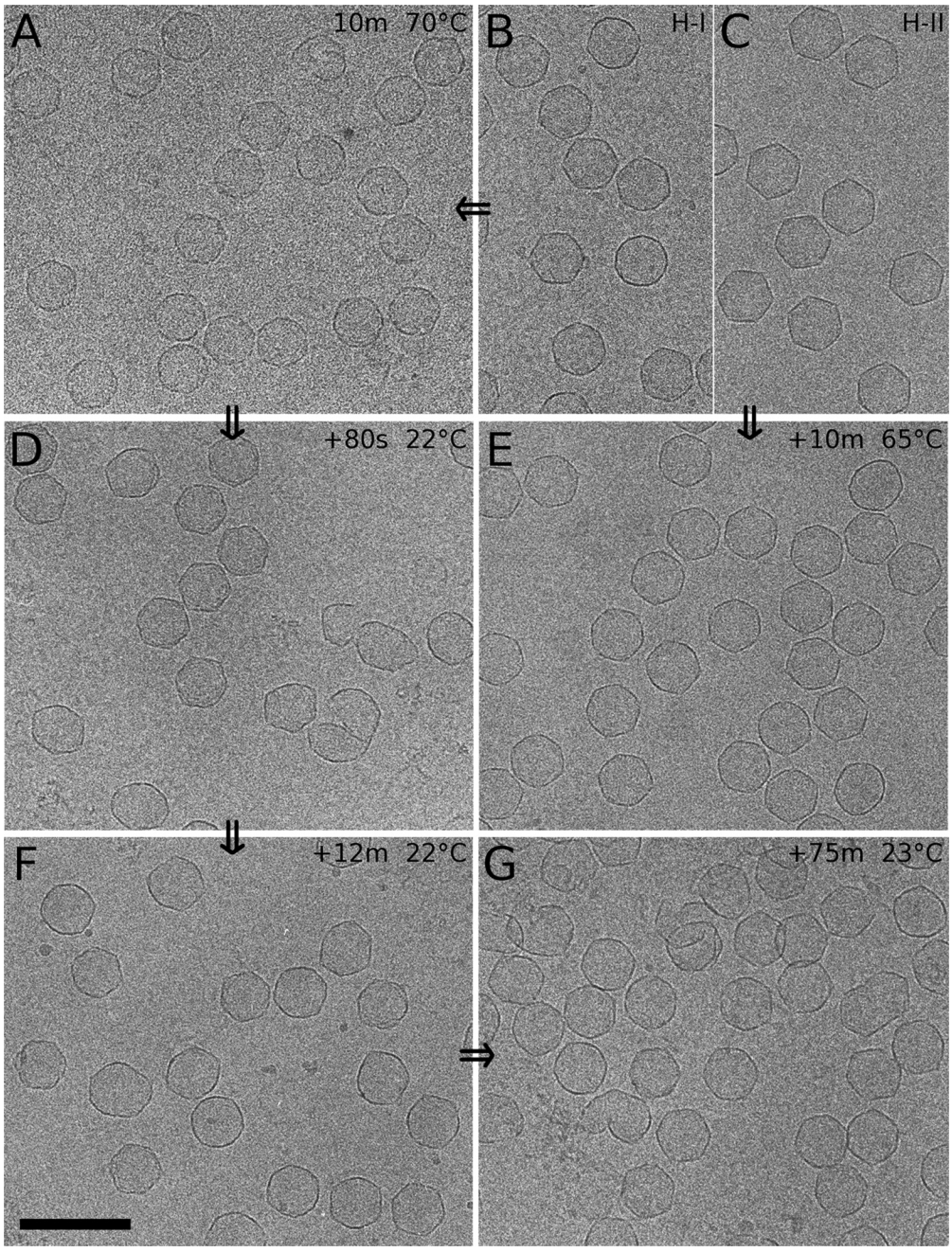

FIG 2 Cryo-electron micrographs showing fields of Head I before (B) and after (A) incubation at 70°C and at various time points after restoration to room temperature (22°C) (D, F, and G). Also shown is Head II before and after a high-temperature incubation (C and E).

Previous calorimetric experiments determined that the 60° event is reversible, i.e., if Head I is incubated at a temperature above 60°C and then cooled and subsequently rescanned, it again exhibits the same event (25). In the present study, we investigated the time course of reversion. To do so, we transferred a sample of Head I to a 20°C water bath after heating it at 65°C for 10 min and then vitrified samples for cryo-EM at various time points from 80 s out to 75 min. A consistent feature of the cooled samples was a much higher incidence of visibly distorted or ruptured particles (Fig. 2D, F, and G) than in either the starting material (Fig. 2B) or the heated sample (Fig. 2A).

To quantitate these observations, we measured the average diameters of several hundred capsids from each sample. The mean and standard deviation for each sample are plotted in Fig. 3. We also measured the percentage of regular capsids (P_r) for each time point (red data points in Fig. 3) and hence the percentages of ruptured or distorted capsids ($100 - P_r$). By 12 min of cooling, the capsids had all reverted to their original conformation, as judged by the diameters and appearance of the regular capsids and by the smooth surface and thin walls of the distorted/ruptured capsids. The incidence of distorted/ruptured capsids at later time points remained consistently about 55%, approximately 5-fold higher

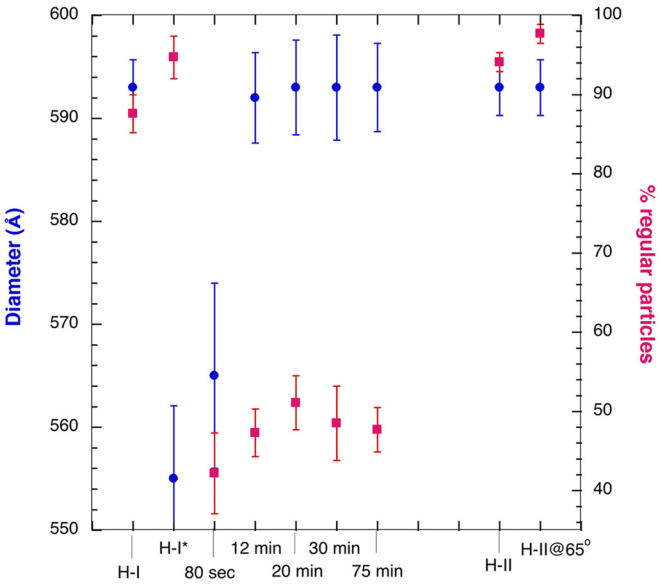

FIG 3 Diameters of regular capsids and percentages of regular (nondistorted) HK97 capsids under various conditions. The diameter data are in blue, and the percentages are in red.

than in the control sample. Because the percentage of regular capsids in the heated sample was no lower than that in the starting material, the observed deformations must have been sustained during cooling as the capsids attempted to revert to their original conformational state.

An atypically large standard deviation in a set of diameter measurements would suggest that more than one structural species was present. Such was the case for the regular capsids captured after 80 s of cooling, which also appear to be intermediate in average diameter between the heated sample and the control (Fig. 3). Computational classification of 1,025 randomly chosen regular capsids indicated that they consisted of ~80% Head I* and ~20% Head I. These data suggest that reversion is triggered with a half-life of ~3 min under these experimental conditions.

In order to ascertain whether the Head I-to-Head I* transition would be affected by cross-linking, we subjected a preparation of purified Head II (the mature, cross-linked, wild-type capsid) to the same treatment. These capsids remained unchanged in size and in their low incidence of distorted particles (Fig. 2C and E and 3). Thus, cross-linking blocks this transition. As Head II does not exhibit a 60° endotherm (25), this finding confirmed the correlation between that endotherm and the structural transition of Head I.

To examine the conformational change, we calculated a three-dimensional (3D) reconstruction of Head I*. The resolution of this density map (Fig. 4A) was 12.9 Å. Normally, we would expect somewhat higher resolution for HK97 capsids with data in this amount and of this quality (as assessed from the spectral limit of Fourier transforms of the scanned micrographs), and indeed, 10.6 Å was achieved in a parallel analysis of Head I. This shortfall in resolution may indicate a microheterogeneity in Head I* structures, such as small departures from icosahedral symmetry that are not evident by visual appraisal. Notwithstanding, the reconstruction clearly shows Head I* to be ~7% smaller than Head I (625 Å versus 670 Å in diameter, vertex to vertex) and rounder (cf. Fig. 4A and B). Of note, Head I* is the same size as the EI (14) and Prohead I* (27) capsids, but direct comparison with the latter particles (see Fig. S2 in the supplemental material) shows that they represent significantly different conformations; see, for instance, the indentation at the 2-fold axis of Head I* (arrowhead in Fig. 4A), which is not present in the other two particles.

In order to interpret the density map of Head I* in greater detail, we performed "flexible fitting," starting from the crystal structure of Head I. The resulting model fits essentially perfectly into the density map (Fig. 5A and B). It identifies the changes undergone by gp5* subunits that produce the observed shrinkage

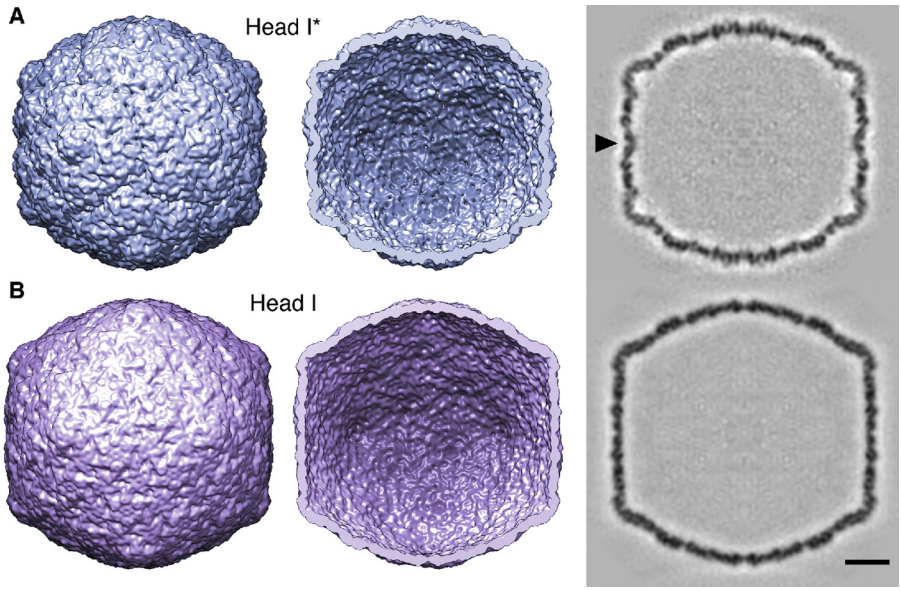

FIG 4 Cryo-EM reconstructions of Head I* (A) and Head I (B), viewed along a 2-fold symmetry axis. (Left) Outer surfaces; (middle) inner surfaces; (right) central sections. The arrowhead in panel A (right panel) points to a distinctive indentation at the 2-fold axis. Bar, 10 nm.

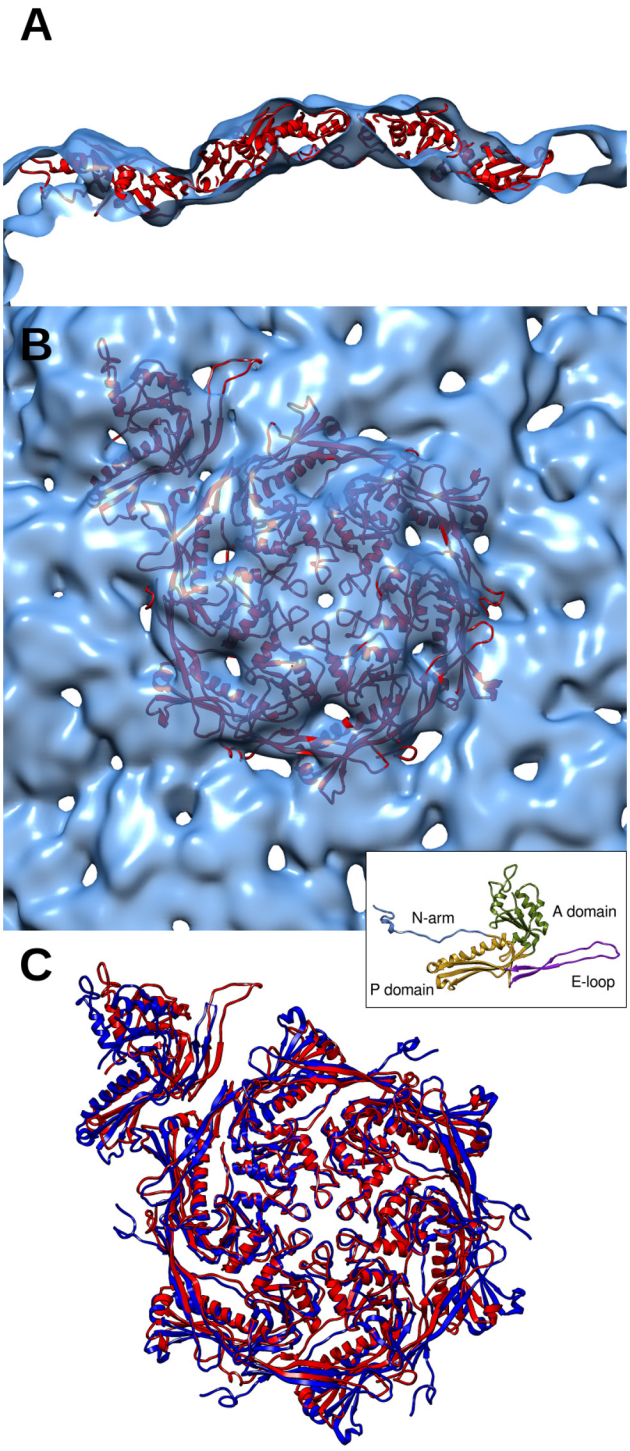

FIG 5 Flexible fitting and molecular modeling of the asymmetric unit (one hexamer plus one pentamer subunit) of Head I*. The fit of the resulting pseudoatomic model into the cryo-EM reconstruction is illustrated in panels A and B. (A) Side view through a cross-sectional slab. (B) Top view from the outside. The inset at bottom right is a ribbon diagram showing the main features of the subunit fold (Head II conformation). (C) Ribbon diagrams of Head I (red; PDB ID 2FS3) and Head I* (blue; after flexible fitting) are compared.

of the capsid. These changes are most easily appraised from movies simulating the transition (see Movies S1 to S4 in the supplemental material). The pentamer shows no significant changes in tertiary structure, although it undergoes an inward radial movement (the model appears to show a change in the pentamer E-loop [Fig. 5C; see also Movie S2], but we do not assign significance to this as this E-loop was arbitrarily modeled in Head I, its coordinates not being defined in the atomic model). On the other hand, the hexamer undergoes several modifications, the most notable being a reduction in diameter from ~158 Å to ~151 Å. This reduction is achieved by the P- and A-domains moving closer to each other, through a rotation of ~10° about the residues linking the two domains. Each E-loop, sitting above the P-domain of the adjacent subunit (see Movie S2), maintains that relative position. In the model, the N-arm appears to swivel into a position closer into the hexamer, although its extended structure and the limited resolution of the reconstruction make a firm conclusion difficult. Finally, the angle between the pentamer and the surrounding hexamers is increased slightly, giving the capsid a rounder appearance. In sum, the observed shrinkage of the capsid is achieved by a compaction of the hexamers involving a relative movement of the A- and P-domains and a small change in relative orientation between pentamers and hexamers.

DISCUSSION

Each capsid conformation corresponds to a local minimum in a free energy landscape. As noted above (introduction), its energy receives contributions from subunit folding, subunit association into capsomers (hexamers and pentamers), and assembly of the capsomers. In the HK97 system, the conformational changes primarily involve subunit rotations. In this scenario, the initial conformation represents a relatively high-energy but kinetically accessible state, and as it matures, the capsid proceeds along a pathway of staging posts through the energy landscape. According to the free energy cascade hypothesis (27), these staging posts are at progressively lower energies. However, alternative off-pathway conformations are also possible.

Comparison of Head I* with Prohead I*: revision of the free energy cascade hypothesis. In Prohead I*, the thermally excited variant of Prohead I, the hexamers are in their EI conformation, although their gp5 is still uncleaved (27) (Fig. 1). Prohead I* has the same diameter as EI, whose protein is cleaved (gp5*). Head I* also has the same diameter as EI, and it has cleaved gp5*. Both thermally induced transitions are reversible, but Prohead I* reverts ~500 times more rapidly than Head I*, when cooled.

It is striking that the capsid switches to the same intermediate diameter when heated, regardless of whether that size is attained by expansion (of Prohead I) or shrinkage (of Head I). It follows that this diameter corresponds to a particularly stable conformation or, more precisely, three similar (but nonidentical) conformations. The one arrived at depends on a specimen's history: for example, Head I* is reached only from the Head I starting point. It appears that Head I* represents a lower-free-energy state than Head I, but there is a kinetic barrier between the two states that is not passed unless there is an infusion of thermal energy (Fig. 6A). In turn, Head I has a lower denaturation temperature (T_m, 83°C) than does Prohead II (T_m, 84.5°C) (25). (The present observations indicate that the former T_m actually refers to Head I*: it is not clear how the T_m of Head I could be measured.) Thus, if the capsids are

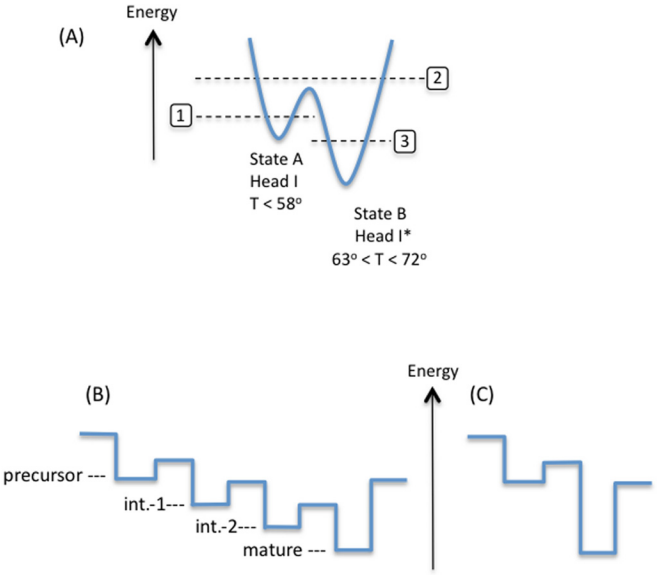

FIG 6 Schematic diagram of energetic transactions involved in conformational changes of a capsid. (A) There are two states fairly close in the energy landscape, of which the one at right (state B) is a lower-energy state, but the one at left (state A) is kinetically more accessible (level 1). A particle may switch from A to B upon heating, which overcomes the barrier between the two states (level 2), from which it may relax into state B (level 3). (B and C) A large conformational change is alternatively accomplished in three subtransitions via intermediates 1 and 2 (B) or in a single step (C).

listed in descending order according to thermal stability, they appear as Prohead II > Head I* > Head I.

At first sight, this ordering appears contrary to the free energy cascade hypothesis (26), which assigns more-mature conformations to lower-free-energy (i.e., more-stable) states (Head I represents the endpoint of a maturation pathway, and Head I* resembles an intermediate [EI-like] stage, later than Prohead II). This conundrum may be resolved by recognizing that the wild-type maturation pathway involves factors other than the structure of the protein shell. One is the cross-links whose formation, starting in EI, drives maturation onwards by a Brownian ratchet-like mechanism (25, 28). A second is the packaging of DNA which imposes outward pressure on the capsid wall, presumably driving the system toward structures with greater internal capacity, e.g., favoring Head over EI.

Structural intermediates as stepping stones on maturation pathways. A greatly increased incidence of distorted/ruptured capsids is observed after cooling Head I* (Fig. 2 and 3). It follows that the Head I*-to-Head I transition is not fully reversible, at least in terms of overall structure. This observation also suggests a rationalization for the existence of metastable, icosahedrally symmetric, intermediate particles.

First, let us consider the extent to which icosahedral symmetry may be maintained as a capsid matures. It seems unlikely (to us) that its 60 asymmetric units can somehow be physically coordinated so as to remain identical in conformation throughout maturation. In the same vein, coarse-grained molecular dynamics calculations have suggested that the slowest modes of vibration of HK97 capsids should be asymmetric (29). More plausible is a sequence of icosahedrally symmetric conformations, with the symmetry requirement being relaxed in the transitions between successive states. For instance, a transition may initiate locally at some site or sites and propagate over the entire surface. Indeed, such a mechanism has been explicitly proposed (30). To date, there have been only a few observations of capsids with different regions having clearly different structures, but precedents have been set in maturing giant capsids of phage T4 (31, 32) and rubella virus (33). The paucity of such observations suggests that the putative subtransitions, once triggered, tend to be rapid. However, the relatively low resolution of our Head I* reconstruction (discussed above) raises the possibility that there may also be other departures from icosahedral symmetry that are less conspicuous than the gross distortions but nevertheless sufficient to limit the resolution of this reconstruction. A similar phenomenon may underlie the empirical fact that in cryo-EM reconstructions of capsids generally, the data sets are found to contain subsets of images that do not fit cohesively with the rest of the data set and are rejected for that reason.

In principle, a wave-like propagation mechanism threatens the integrity of the maturing particle. At the wave front, the subunits in a given capsomer are in different, nonequivalent, local environments, and as their core domains rotate, there must be a point at which the intercapsomer contacts are weakened if not disconnected. If such faults were to propagate along lattice lines, rupture or distortion of the capsid would be possible if not probable. The risk of damage may depend on the location of the initiation site: for instance, it may be lower in a vertex than in a less symmetrically positioned site on a facet. Moreover, the risk appears to depend on the transition in question, at least in the HK97 system, where the Head I-to-Head I* transition is low risk but the Head I*-to-Head I transition is high risk.

We posit that, in general, the likelihood of such a catastrophe is greater the larger the conformational difference between the "before" and "after" states, and conversely. Thus, the likelihood of a successful outcome (an intact mature capsid) should be enhanced by breaking the overall transformation down into several smaller, relatively low-risk steps (Fig. 6B and C). Hence, it should be beneficial to have one or more icosahedrally symmetric intermediates to serve as stepping stones along the maturation pathway.

Intermediates in other viral systems. How widespread are metastable transition states of maturing capsids? Assessment is constrained by the fact that pertinent data are available for only a few viruses. However, it is clear that the HK97 system is not unique in this respect. Similar behavior has been observed in the maturation pathway of the double-stranded RNA (dsRNA) bacteriophage ϕ6 (34). Despite having a capsid protein fold and procapsid morphology different from those of HK97 (35, 36), this capsid also undergoes radical structural changes as it matures (1). These changes also involve subunit rotations, and there are two intermediates. Of these, the second is the lowest-energy state for the empty capsid, with the mature capsid structure being reached only after the genome has been packaged, and pushes the capsid wall out into its final spherical shape. If the genome is lost, the capsid reverts to a polyhedral intermediate conformation (34). Moreover, the maturing capsid of herpes simplex virus, which is based on a core domain with an HK97-like fold (15), passes through multiple icosahedrally symmetric intermediates (37), and NωV, a T=4 insect virus, passes through a near-continuum of intermediate states as it undergoes acid-induced maturation (38, 39).

On the other hand, intermediates may not be universal, as the T5 capsid has been reported to switch directly from its precursor conformation to its mature conformation (40). However, some such states may be short-lived and consequently difficult to detect. It may also be that there is more than one molecular mechanism

that mediates this process (damage-free maturation), as with the stabilization mechanisms compared in the introduction. Thus, one such pathway involves stepping through intermediates, while, in another, the capsid protein has evolved to be able to mature securely without requiring intermediates.

MATERIALS AND METHODS

Preparation of Head I. Head I and Head II were made by expanding purified wild-type Prohead II or Prohead II-K169Y (19, 20) *in vitro*. Both were prepared as previously described for the wild-type particles (18, 41). The two variants of gp5 were coexpressed with the HK97 protease from plasmid pV0 (pT7-5Hd2.9) for wild type (19) or from plasmid pV0-K169Y (18) for the mutant. Proheads were purified from cell lysates by polyethylene glycol precipitation, differential centrifugation, velocity sedimentation in glycerol gradients, and ion-exchange chromatography on a Poros HQ20 (ABI, Foster City, CA) column using a BioCad Sprint system (ABI, Foster City, CA). The Proheads were matured by the same urea/low-pH method previously used to make Head II for X-ray crystallographic studies (19, 20, 42). Before starting the expansion reaction, the capsids were diluted to ~10 mg/ml in 0.2 M KCl in the presence of 1 mM 2-mercaptoethanol to avoid aggregation. Then, they were treated with 7 M urea in pH 5 buffer (50 mM sodium acetate) at 20°C for 1 h before being diluted 20-fold into a neutralizing buffer (50 mM Tris-HCl, pH 7.5) and dialyzed exhaustively at 4°C to remove the urea. The final sample was concentrated by ultracentrifugation, and the pellet was resuspended in calorimetry buffer (0.1 M KCl, 0.02 M KPO_4, pH 7.5).

Thermo-cryo-EM. To vitrify particles for cryo-EM observation from defined conditions of elevated temperature and humidity, we used a custom-made environmental chamber that mounts over a cryo-station (see Fig. S1 in the supplemental material). In brief, 3-μl drops of specimen were applied to EM grids mounted within the chamber, incubated for 10 min at 65°C or 70°C, and then blotted to thin films and vitrified in an otherwise conventional manner. Finally, grids were transferred into the electron microscope and low-dose micrographs were recorded on a CM200-FEG electron microscope (FEI, Hillsboro, OR) equipped with a Gatan 626 cryo-holder using procedures previously described (43). The Head I* sample was imaged at a magnification of ×38,000 and defocus values in the range of 0.78 μm to 2.15 μm. Films were digitized with a Zeiss SCAI scanner with a 7-μm sampling rate to yield 1.84 Å/pixel at the sample. The Head I sample was imaged at a magnification of ×50,000, and films were scanned on a Nikon Super CoolScan 9000 scanner with a 6.35-μm sampling rate, yielding 1.27 Å/pixel. Capsid diameters were measured by hand as averages of three measurements at positions 60° apart for each capsid. To estimate the incidence of damaged capsids, ~400 capsids from three representative micrographs were scored independently for each sample by two observers.

Image reconstruction. Capsid images were boxed out from digitized micrographs using x3dpreprocess (44). Contrast transfer functions were estimated with Bsoft (45), and corrections were applied during orientation refinement and image reconstruction with AUTO3DEM (46). Initial models were calculated *de novo* using the RMC method (47). For the Head I* reconstruction, 4,654 capsid images were picked and the best (highest-correlating) 2,314 images yielded a density map with 12.9-Å resolution, according to the Fourier shell correlation (FSC) criterion with an 0.5 threshold. For the control Head I reconstruction, the corresponding numbers were 4,897 total images, 2,445 reconstructed, and 10.6-Å resolution. To ensure a fair comparison in Fig. 4, the resolution of the control Head I map was limited to match that of the Head I* map.

Pseudoatomic modeling. A model consisting of seven gp5* subunits arranged in the asymmetric unit of an icosahedral capsid was obtained by a flexible fitting procedure. The atomic coordinates from the crystal structure of Head I (Protein Data Bank [PDB] identifier [ID] 2FS3) (48) were taken as the initial model, after modeling in the E-loop (residues 159 to 171) that is missing from the pentamer subunit. The seven subunits were then fitted manually, as a single rigid body, into the cryo-EM density of the reconstruction, using the "fit in map" tool in Chimera (49). This model was refined iteratively, using the molecular dynamics flexible fitting (MDFF) procedure (50), complying with the symmetry constraints of the capsid without having to model more than one asymmetric unit. Ten iterations were performed in total. Before each of the first eight iterations, the current coordinates for one asymmetric unit were used to extend the model by adding the five closest neighboring units (tool *Sym* in Chimera). The reconstructed density corresponding to each unit of this extended model was then segmented separately (tools Color *Zone* and Split *Map* in Chimera), and the portion corresponding to the central asymmetric unit was filtered to 13 Å, i.e., the nominal resolution of the map (*bfilter* in Bsoft [45]) and set as the target density for flexible fitting. Then, a molecular dynamics simulation of 50 ps was run *in vacuo* using the MDFF program that is part of NAMD (51), with the density providing an additional force field. To limit the degrees of freedom in the simulation, the secondary structure of the model was preserved. In the last two iterations, the boundaries of the model were refined by performing 2,000 iterations of energy minimization on the composite model containing the latest solution and copies of the 5 surrounding neighboring units, with the corresponding density being resegmented after each iteration to provide an additional force field. Finally, the coordinates of the central asymmetric unit defined our pseudoatomic model of Head I*.

SUPPLEMENTAL MATERIAL

Supplemental material for this article may be found at http://mbio.asm.org/lookup/suppl/doi:10.1128/mBio.02067-14/-/DCSupplemental.

Figure S1, PDF file, 5.4 Mb.
Figure S2, PDF file, 4.0 Mb.
Movie S1, MP4 file, 4.0 Mb.
Movie S2, MP4 file, 4.0 Mb.
Movie S3, MP4 file, 4.0 Mb.
Movie S4, MP4 file, 4.0 Mb.

ACKNOWLEDGMENTS

We thank Gary Melvin and Dennis Winkler for designing and constructing our environmental chambers.

This work was supported by the Intramural Research Program of NIAMS and by NIH grant R01 GM047795 to R.W.H.

REFERENCES

1. **Butcher SJ, Dokland T, Ojala PM, Bamford DH, Fuller SD.** 1997. Intermediates in the assembly pathway of the double-stranded RNA virus phi6. EMBO J. **16:**4477–4487. http://dx.doi.org/10.1093/emboj/16.14.4477.
2. **Mukhopadhyay S, Kuhn RJ, Rossmann MG.** 2005. A structural perspective of the flavivirus life cycle. Nat. Rev. Microbiol. **3:**13–22. http://dx.doi.org/10.1038/nrmicro1067.
3. **Steven AC, Heymann JB, Cheng N, Trus BL, Conway JF.** 2005. Virus maturation: dynamics and mechanism of a stabilizing structural transition that leads to infectivity. Curr. Opin. Struct. Biol. **15:**227–236. http://dx.doi.org/10.1016/j.sbi.2005.03.008.
4. **Sundquist WI, Kräusslich HG.** 2012. HIV-1 assembly, budding, and maturation. Cold Spring Harb. Perspect. Med. **2:**a006924. http://dx.doi.org/10.1101/cshperspect.a006924.
5. **Cardone G, Heymann JB, Cheng N, Trus BL, Steven AC.** 2012. Procapsid assembly, maturation, nuclear exit: dynamic steps in the production of infectious herpesvirions. Adv. Exp. Med. Biol. **726:**423–439. http://dx.doi.org/10.1007/978-1-4614-0980-9_19.
6. **Steven AC, Greenstone HL, Booy FP, Black LW, Ross PD.** 1992. Conformational changes of a viral capsid protein. Thermodynamic rationale for proteolytic regulation of bacteriophage T4 capsid expansion, cooperativity, and super-stabilization by soc binding. J. Mol. Biol. **228:**870–884. http://dx.doi.org/10.1016/0022-2836(92)90871-G.
7. **Ishii T, Yanagida M.** 1977. The two dispensable structural proteins (soc and hoc) of the T4 phage capsid; their purification and properties, isolation and characterization of the defective mutants, and their binding with the defective heads *in vitro*. J. Mol. Biol. **109:**487–514. http://dx.doi.org/10.1016/S0022-2836(77)80088-0.

8. **Sternberg N, Weisberg R.** 1977. Packaging of coliphage lambda DNA. II. Role gene D protein. J. Mol. Biol. **117:**733–759.
9. **Yang F, Forrer P, Dauter Z, Conway JF, Cheng N, Cerritelli ME, Steven AC, Plückthun A, Wlodawer A.** 2000. Novel fold and capsid-binding properties of the lambda-phage display platform protein gpD. Nat. Struct. Biol. **7:**230–237. http://dx.doi.org/10.1038/73347.
10. **Duda RL.** 1998. Protein chain mail: catenated protein in viral capsids. Cell **94:**55–60. http://dx.doi.org/10.1016/S0092-8674(00)81221-0.
11. **Galisteo ML, King J.** 1993. Conformational transformations in the protein lattice of phage P22 procapsids. Biophys. J. **65:**227–235. http://dx.doi.org/10.1016/S0006-3495(93)81073-7.
12. **Parent KN, Khayat R, Tu LH, Suhanovsky MM, Cortines JR, Teschke CM, Johnson JE, Baker TS.** 2010. P22 coat protein structures reveal a novel mechanism for capsid maturation: stability without auxiliary proteins or chemical crosslinks. Structure **18:**390–401. http://dx.doi.org/10.1016/j.str.2009.12.014.
13. **Agirrezabala X, Martín-Benito J, Castón JR, Miranda R, Valpuesta JM, Carrascosa JL.** 2005. Maturation of phage T7 involves structural modification of both shell and inner core components. EMBO J. **24:**3820–3829. http://dx.doi.org/10.1038/sj.emboj.7600840.
14. **Lata R, Conway JF, Cheng N, Duda RL, Hendrix RW, Wikoff WR, Johnson JE, Tsuruta H, Steven AC.** 2000. Maturation dynamics of a viral capsid: visualization of transitional intermediate states. Cell **100:**253–263. http://dx.doi.org/10.1016/S0092-8674(00)81563-9.
15. **Baker ML, Jiang W, Rixon FJ, Chiu W.** 2005. Common ancestry of herpesviruses and tailed DNA bacteriophages. J. Virol. **79:**14967–14970. http://dx.doi.org/10.1128/JVI.79.23.14967-14970.2005.
16. **Homa FL, Huffman JB, Toropova K, Lopez HR, Makhov AM, Conway JF.** 2013. Structure of the pseudorabies virus capsid: comparison with herpes simplex virus type 1 and differential binding of essential minor proteins. J. Mol. Biol. **425:**3415–3428. http://dx.doi.org/10.1016/j.jmb.2013.06.034.
17. **Steven AC, Spear PG.** 1997. Herpesvirus capsid assembly and envelopment, p 3123415–351. *In* Chiu W, Burnett RM, Garcea RL (ed), Structural biology of viruses. Oxford University Press, New York, NY.
18. **Duda RL, Martincic K, Hendrix RW.** 1995. Genetic basis of bacteriophage HK97 prohead assembly. J. Mol. Biol. **247:**636–647. http://dx.doi.org/10.1006/jmbi.1994.0169.
19. **Duda RL, Hempel J, Michel H, Shabanowitz J, Hunt D, Hendrix RW.** 1995. Structural transitions during bacteriophage HK97 head assembly. J. Mol. Biol. **247:**618–635. http://dx.doi.org/10.1006/jmbi.1995.0168.
20. **Conway JF, Duda RL, Cheng N, Hendrix RW, Steven AC.** 1995. Proteolytic and conformational control of virus capsid maturation: the bacteriophage HK97 system. J. Mol. Biol. **253:**86–99. http://dx.doi.org/10.1006/jmbi.1995.0538.
21. **Hendrix RW, Johnson JE.** 2012. Bacteriophage HK97 capsid assembly and maturation. Adv. Exp. Med. Biol. **726:**351–363. http://dx.doi.org/10.1007/978-1-4614-0980-9_15.
22. **May ER, Feng J, Brooks CL III.** 2012. Exploring the symmetry and mechanism of virus capsid maturation via an ensemble of pathways. Biophys. J. **102:**606–612. http://dx.doi.org/10.1016/j.bpj.2011.11.3302.
23. **Gertsman I, Gan L, Guttman M, Lee K, Speir JA, Duda RL, Hendrix RW, Komives EA, Johnson JE.** 2009. An unexpected twist in viral capsid maturation. Nature **458:**646–650. http://dx.doi.org/10.1038/nature07686.
24. **Veesler D, Quispe J, Grigorieff N, Potter CS, Carragher B, Johnson JE.** 2012. Maturation in action: CryoEM study of a viral capsid caught during expansion. Structure **20:**1384–1390. http://dx.doi.org/10.1016/j.str.2012.05.011.
25. **Ross PD, Cheng N, Conway JF, Firek BA, Hendrix RW, Duda RL, Steven AC.** 2005. Crosslinking renders bacteriophage HK97 capsid maturation irreversible and effects an essential stabilization. EMBO J. **24:**1352–1363. http://dx.doi.org/10.1038/sj.emboj.7600613.
26. **Ross PD, Conway JF, Cheng N, Dierkes L, Firek BA, Hendrix RW, Steven AC, Duda RL.** 2006. A free energy cascade with locks drives assembly and maturation of bacteriophage HK97 capsid. J. Mol. Biol. **364:**512–525. http://dx.doi.org/10.1016/j.jmb.2006.08.048.
27. **Conway JF, Cheng N, Ross PD, Hendrix RW, Duda RL, Steven AC.** 2007. A thermally induced phase transition in a viral capsid transforms the hexamers, leaving the pentamers unchanged. J. Struct. Biol. **158:**224–232. http://dx.doi.org/10.1016/j.jsb.2006.11.006.
28. **Lee KK, Gan L, Tsuruta H, Moyer C, Conway JF, Duda RL, Hendrix RW, Steven AC, Johnson JE.** 2008. Virus capsid expansion driven by the capture of mobile surface loops. Structure **16:**1491–1502. http://dx.doi.org/10.1016/j.str.2008.06.014.
29. **Rader AJ, Vlad DH, Bahar I.** 2005. Maturation dynamics of bacteriophage HK97 capsid. Structure **13:**413–421. http://dx.doi.org/10.1016/j.str.2004.12.015.
30. **Cermelli P, Indelicato G, Twarock R.** 2013. Nonicosahedral pathways for capsid expansion. Phys. Rev. E Stat. Nonlin. Soft Matter Phys. **88:**032710. http://dx.doi.org/10.1103/PhysRevE.88.032710.
31. **Steven AC, Carrascosa JL.** 1979. Proteolytic cleavage and structural transformation: their relationship in bacteriophage T4 capsid maturation. J. Supramol. Struct. **10:**1–11. http://dx.doi.org/10.1002/jss.400100102.
32. **Müller M, Mesyanzhinov VV, Aebi U.** 1994. *In vitro* maturation of prehead-like bacteriophage T4 polyheads: structural changes accompanying proteolytic cleavage and lattice expansion. J. Struct. Biol. **112:**199–215. http://dx.doi.org/10.1006/jsbi.1994.1021.
33. **Plevka P, Battisti AJ, Junjhon J, Winkler DC, Holdaway HA, Keelapang P, Sittisombut N, Kuhn RJ, Steven AC, Rossmann MG.** 2011. Maturation of flaviviruses starts from one or more icosahedrally independent nucleation centres. EMBO Rep. **12:**602–606. http://dx.doi.org/10.1038/embor.2011.75.
34. **Nemecek D, Cheng N, Qiao J, Mindich L, Steven AC, Heymann JB.** 2011. Stepwise expansion of the bacteriophage varphi6 procapsid: possible packaging intermediates. J. Mol. Biol. **414:**260–271. http://dx.doi.org/10.1016/j.jmb.2011.10.004.
35. **Nemecek D, Boura E, Wu W, Cheng N, Plevka P, Qiao J, Mindich L, Heymann JB, Hurley JH, Steven AC.** 2013. Subunit folds and maturation pathway of a dsRNA virus capsid. Structure **21:**1374–1383. http://dx.doi.org/10.1016/j.str.2013.06.007.
36. **El Omari K, Sutton G, Ravantti JJ, Zhang H, Walter TS, Grimes JM, Bamford DH, Stuart DI, Mancini EJ.** 2013. Plate tectonics of virus shell assembly and reorganization in phage φ8, a distant relative of mammalian reoviruses. Structure **21:**1384–1395. http://dx.doi.org/10.1016/j.str.2013.06.017.
37. **Heymann JB, Cheng N, Newcomb WW, Trus BL, Brown JC, Steven AC.** 2003. Dynamics of herpes simplex virus capsid maturation visualized by time-lapse cryo-electron microscopy. Nat. Struct. Biol. **10:**334–341. http://dx.doi.org/10.1038/nsb922.
38. **Matsui T, Lander GC, Khayat R, Johnson JE.** 2010. Subunits fold at position-dependent rates during maturation of a eukaryotic RNA virus. Proc. Natl. Acad. Sci. USA **107:**14111–14115. http://dx.doi.org/10.1073/pnas.1004221107.
39. **Matsui T, Tsuruta H, Johnson JE.** 2010. Balanced electrostatic and structural forces guide the large conformational change associated with maturation of T = 4 virus. Biophys. J. **98:**1337–1343. http://dx.doi.org/10.1016/j.bpj.2009.12.4283.
40. **Preux O, Durand D, Huet A, Conway JF, Bertin A, Boulogne C, Drouin-Wahbi J, Trévarin D, Pérez J, Vachette P, Boulanger P.** 2013. A two-state cooperative expansion converts the procapsid shell of bacteriophage T5 into a highly stable capsid isomorphous to the final virion head. J. Mol. Biol. **425:**1999–2014. http://dx.doi.org/10.1016/j.jmb.2013.03.002.
41. **Li Y, Conway JF, Cheng N, Steven AC, Hendrix RW, Duda RL.** 2005. Control of virus assembly: HK97 "Whiffleball" mutant capsids without pentons. J. Mol. Biol. **348:**167–182. http://dx.doi.org/10.1016/j.jmb.2005.02.045.
42. **Wikoff WR, Liljas L, Duda RL, Tsuruta H, Hendrix RW, Johnson JE.** 2000. Topologically linked protein rings in the bacteriophage HK97 capsid. Science **289:**2129–2133. http://dx.doi.org/10.1126/science.289.5487.2129.
43. **Cheng N, Conway JF, Watts NR, Hainfeld JF, Joshi V, Powell RD, Stahl SJ, Wingfield PE, Steven AC.** 1999. Tetrairidium, a four-atom cluster, is readily visible as a density label in three-dimensional cryo-EM maps of proteins at 10-25 Å resolution. J. Struct. Biol. **127:**169–176. http://dx.doi.org/10.1006/jsbi.1999.4120.
44. **Conway JF, Steven AC.** 1999. Methods for reconstructing density maps of "single" particles from cryoelectron micrographs to subnanometer resolution. J. Struct. Biol. **128:**106–118. http://dx.doi.org/10.1006/jsbi.1999.4168.
45. **Heymann JB, Belnap DM.** 2007. Bsoft: image processing and molecular modeling for electron microscopy. J. Struct. Biol. **157:**3–18. http://dx.doi.org/10.1016/j.jsb.2006.06.006.
46. **Yan X, Sinkovits RS, Baker TS.** 2007. AUTO3DEM—an automated and high throughput program for image reconstruction of icosahedral parti-

cles. J. Struct. Biol. **157:**73–82. http://dx.doi.org/10.1016/j.jsb.2006.08.007.

47. **Yan X, Dryden KA, Tang J, Baker TS.** 2007. Ab initio random model method facilitates 3D reconstruction of icosahedral particles. J. Struct. Biol. **157:**211–225. http://dx.doi.org/10.1016/j.jsb.2006.07.013.
48. **Gan L, Speir JA, Conway JF, Lander G, Cheng N, Firek BA, Hendrix RW, Duda RL, Liljas L, Johnson JE.** 2006. Capsid conformational sampling in HK97 maturation visualized by X-ray crystallography and cryo-EM. Structure **14:**1655–1665. http://dx.doi.org/10.1016/j.str.2006.09.006.
49. **Pettersen EF, Goddard TD, Huang CC, Couch GS, Greenblatt DM, Meng EC, Ferrin TE.** 2004. UCSF Chimera—a visualization system for exploratory research and analysis. J. Comput. Chem. **25:**1605–1612. http://dx.doi.org/10.1002/jcc.20084.
50. **Trabuco LG, Villa E, Schreiner E, Harrison CB, Schulten K.** 2009. Molecular dynamics flexible fitting: a practical guide to combine cryo-electron microscopy and X-ray crystallography. Methods **49:**174–180. http://dx.doi.org/10.1016/j.ymeth.2009.04.005.
51. **Phillips JC, Braun R, Wang W, Gumbart J, Tajkhorshid E, Villa E, Chipot C, Skeel RD, Kalé L, Schulten K.** 2005. Scalable molecular dynamics with NAMD. J. Comput. Chem. **26:**1781–1802. http://dx.doi.org/10.1002/jcc.20289.
52. **Duda RL, Ross PD, Cheng N, Firek BA, Hendrix RW, Conway JF, Steven AC.** 2009. Structure and energetics of encapsidated DNA in bacteriophage HK97 studied by scanning calorimetry and cryo-electron microscopy. J. Mol. Biol. **391:**471–483. http://dx.doi.org/10.1016/j.jmb.2009.06.035.